Ship Stability Criteria Based on Chaotic Transients from Incursive Fractals

J. M. T. Thompson, R. C. T. Rainey and M. S. Soliman

Email alerting service	Receive free email alerts when new articles cite this article - sign up in the box at the top right-hand corner of the article or click **here**

Ship stability criteria based on chaotic transients from incursive fractals

By J. M. T. Thompson[1], R. C. T. Rainey[2] and M. S. Soliman[1]

[1] *Department of Civil Engineering, University College London, Gower Street, London WC1E 6BT, U.K.*
[2] *Atkins Engineering Sciences, Woodcote Grove, Epsom, Surrey KT18 5BW, U.K.*

This article surveys some recent findings in the nonlinear dynamics of driven oscillators that appear to offer a new approach to the quantification of ship stability in waves. The major discovery is that in situations where the resonant motions can escape over a local maximum of the potential energy (as in capsize), there is always likely to be a sudden reduction in area of the safe basin of attraction in the space of the starting conditions. This is associated with a gross striation of the basin, and can occur at a forcing magnitude that is a small fraction of that at which the final steady-state motions lose their stability. It is argued that this well-defined basin erosion could form the basis of a new design criterion based on transient motions. This approach has the twin advantages of being both conceptually simpler and at the same time more relevant than one based on a stability analysis of the steady state rolling motions which can be dangerously non-conservative.

Introduction

Recent developments in the field of nonlinear dynamics and chaos seem to play a dual role in the long-standing problem of the capsizing of ships in waves. On the one hand they explain the lack of success of traditional methods of dynamic analysis, by showing that the problem is very much more complicated than hitherto envisaged in the literature of naval architecture. On the other hand they suggest that transient conditions, produced by the sudden arrival of a group of regular waves, and traditionally regarded as hopelessly complicated, may in fact produce highly repeatable capsize behaviour. This could form the basis of a new index of 'capsizability', that might have considerable practical value. It is a paradox that this macroscopic repeatability is the result of chaotic transients from incursive fractals, which are a paradigm of microscopic unpredictability.

In the design office, the stability of a ship is currently judged on the basis of its 'GZ curve', which is a graph of the hydrostatic restoring-moment experienced by the vessel in still water, plotted as a function of the angle of roll. The criteria for 'safety' are at present purely empirical: it is for example specified that the areas (potential energies) under various portions of the graph must exceed certain internationally agreed figures, which have been found over the years to ensure acceptable stability performance. It is, however, acknowledged in the naval architecture literature (see, for example, the numerous relevant papers in Motora (1982)) that this procedure is inherently unsatisfactory because it ignores the contributions made by dynamic parameters, such as the important roll damping. To incorporate these parameters, a

series of attempts have been made to idealize a ship as a harmonically excited nonlinear spring–mass–damper system, and to analyse its stability by the classical methods of analytical dynamics using, for example, harmonic balance methods, perturbation schemes and Liapunov functions: this can again be seen in Motora (1982). The hopeless complexity and ultimate irrelevance of all steady-state analyses is clearly established by recent studies of a canonical oscillator that we shall describe in this review.

Basic equation of rolling motion

By way of illustration, we consider here the modelling of a boat as a single degree-of-freedom, non-linear oscillator. We should emphasize, however, that our conclusions are completely general. They apply to realistic computer models of ships in a seaway, using, for example, developments in hydrodynamic strip theory (Rainey 1989, 1990) and, perhaps most crucially, to the physical models used in wave-tank testing. The rolling motions of a boat in regular beam seas will be modelled then, most basically, by an equation of the form,

$$I\theta'' + B(\theta') + C(\theta) = D\sin(w\tau), \tag{1}$$

where the angle of roll $\theta(\tau)$ is sometimes measured in a fixed reference frame, and sometimes relative to the wave slope: a prime denotes differentiation with respect to the real (unscaled) time τ. The rotational moment of inertia, I, will normally include added-mass contributions from the surrounding fluid. The damping function $B(\theta')$ will depend crucially on the cross-sectional profile of the vessel, and will often be highly nonlinear (see, for example, Lloyd 1989), modelled, for example, by an expansion of the form $\theta' + \theta'|\theta'| + \theta'^3$: here the modulus in the quadratic term is needed to ensure that the damping moment always opposes the instantaneous angular velocity.

The restoring moment, $C(\theta)$, of the buoyancy forces (less any overturning moments due to wind or cargo imbalance) is also highly nonlinear, dropping to zero at an angle of 'vanishing stability', θ_v, where the corresponding potential energy,

$$V(\theta) = \int C(\theta)\,d\theta,$$

has a local maximum. We shall assume throughout that θ is measured from the stable equilibrium state in still water, which in the presence of wind loading might be at a small angle to the vertical. In naval architecture the basic buoyancy function, $C(\theta)$, in the absence of wind and cargo imbalance is invariably called the GZ curve, the distance GZ on a diagram of a rolling boat being the lever arm of the buoyancy force about the centre of gravity. To convert a ship's GZ into a righting moment we must therefore multiply by the weight of the vessel.

The periodic overturning moment due to regular lateral ocean waves can usually be written as $D\sin(w\tau)$, where w is the encounter frequency and D will in general be a function both of the wave height, H, and the frequency w.

Fundamental ratios and non-dimensional form

To facilitate comparisons between different vessels, it is convenient to transform equation (1) into a standard non-dimensional form. We scale the angle to make the positive angle of vanishing stability equal to unity, and we scale the time to make the natural frequency of free linear undamped vibrations of the boat equal to unity.
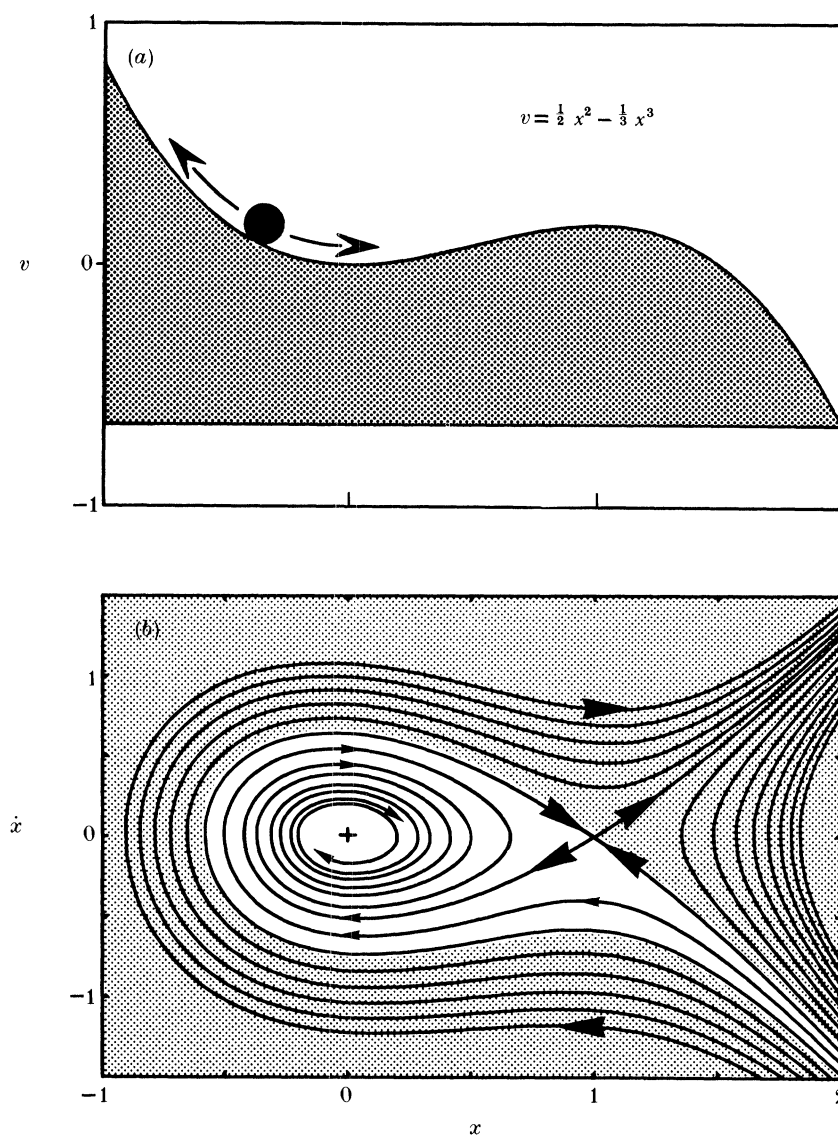
Figure 1. Escape from the canonical potential well, showing (*a*) the cubic potential, and (*b*) the phase portrait of the undriven autonomous system with $F = 0$ and $\beta = 0.1$.

In terms of the new scaled angle, x, and the new scaled time, t, the equation of motion can then be written as,

$$\ddot{x} + b(\dot{x}) + c(x) = F\sin(\omega t), \qquad (2)$$

where a dot denotes differentiation with respect to the new scaled time t. The new restoring function $c(x)$ vanishes at $x = 0$ and at $x = 1$, and has unit slope at the origin: to get it from a naval GZ curve we can simply scale the horizontal axis so that the angle of vanishing stability is at unity, and scale the vertical axis so that the slope at the origin is unity, thereby circumventing any problems with units.

It is finally useful to identify three fundamental ratios (which by their invariant nature will have remained unchanged during the transformation of the equation of

motion). The frequency ratio between the forcing and natural frequencies, is now simply ω. The damping ratio is the conventional one of linear vibration theory, which is here equal to one half of the linear coefficient within an expansion of $b(\dot{x})$.

To define a suitable forcing ratio, we would want to divide F by a representative magnitude of $c(x)$. No such forcing ratio will be needed in the present study, but some remarks on the choice of the representative magnitude might be appropriate. One possibility would be the maximum value of c in the interval $0 < x < 1$. But we feel there is some advantage in taking the average value of c in this interval, c_a, which in the new coordinates is numerically equal to the height of the potential barrier. The forcing ratio would then be F/c_a.

A parametrized family of GZ curves

Restoring-moment curves are often written as polynomials, and it is useful to consider for a moment the family, parametrized by α,

$$c(x) = \mathrm{d}v/\mathrm{d}x = x(1-x)(1+\alpha x), \tag{3}$$

where $v(x)$ is the corresponding potential energy. Potential energy curves are often called curves of 'dynamic stability' in the naval literature, but we prefer not to adopt this rather unusual terminology here. Points of 'vanishing stability', where $c = \mathrm{d}v/\mathrm{d}x = 0$, are at $x = 1$ and at $x = -1/\alpha$.

The case of $\alpha = 1$ corresponds to a symmetric ship with no wind or cargo imbalance: the potential energy has equal barriers at $x = \pm 1$, and there is an equal possibility of capsizing to port or starboard. As α is decreased towards zero, the barrier at negative x gets progressively higher and further from the origin, corresponding to a wind blowing towards positive x, and capsize towards negative x becomes increasingly unlikely.

In a high wind (which would naturally be a component of any worst-case scenario), capsize towards it can be totally discounted, and it is tempting to adopt the limiting case of $\alpha = 0$ in which $c(x)$ is a parabola and $v(x)$ is a simple cubic. This is in fact the canonical cubic potential for which we first observed the dramatic basin erosion in our fundamental investigations of the escape from a potential well (Thompson 1989; Thompson & Ueda 1989; Soliman & Thompson 1989), which we summarize in the following section. For comparisons with the nonlinear dynamics literature, it is worth observing that $\alpha = -0.5$ generates the extensively studied twin-well potential (see for example, the paper by Ueda *et al.* 1990), with two equal wells symmetrically disposed about a central energy barrier. We shall return to this twin-well oscillator in a later section.

Escape from a canonical potential well

The concept of basin erosion, on which our new approach to ship capsize is based, derives from the work of Thompson (1989) on the driven oscillator:

$$\ddot{x} + \beta\dot{x} + x - x^2 = F\sin(\omega t). \tag{4}$$

Here the parabolic restoring force $x - x^2$ drops to zero at $x = 1$, where the total potential energy $v = \frac{1}{2}x^2 - \frac{1}{3}x^3$ has a local maximum. The escape over this canonical cubic potential barrier corresponds to capsize, this equation being in a sense the simplest archetypal capsize model with x as a normalized roll angle (it corresponds to a biased boat under wind loading, as we have described). A dot denotes differentiation with respect to the time, t, and we shall write $\dot{x} \equiv y$.
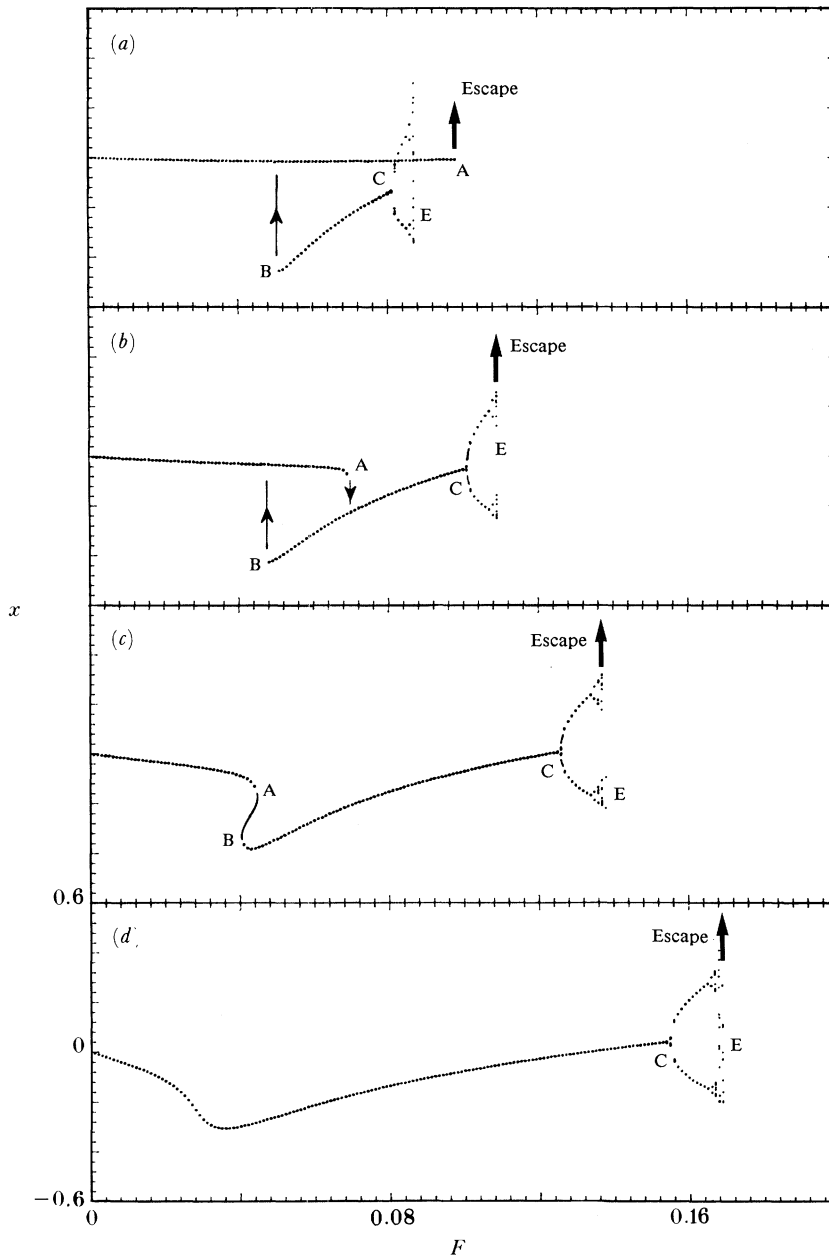
Figure 2. Steady-state escape scenarios under slowly increasing F at four values of the driving frequency ω: (a) 0.80; (b) 0.85; (c) 0.90; (d) 0.95. Here the x coordinate is sampled stroboscopically at the driving period and damping is constant at $\beta = 0.1$.

Figure 1 shows the form of $v(x)$ and the response of the unforced system, with $F = 0$, in the (x, y) phase space. Of particular relevance here is the basin of attraction of the stable equilibrium state at $(0, 0)$, shown in white and bounded by the inset of the unstable hill-top saddle point.
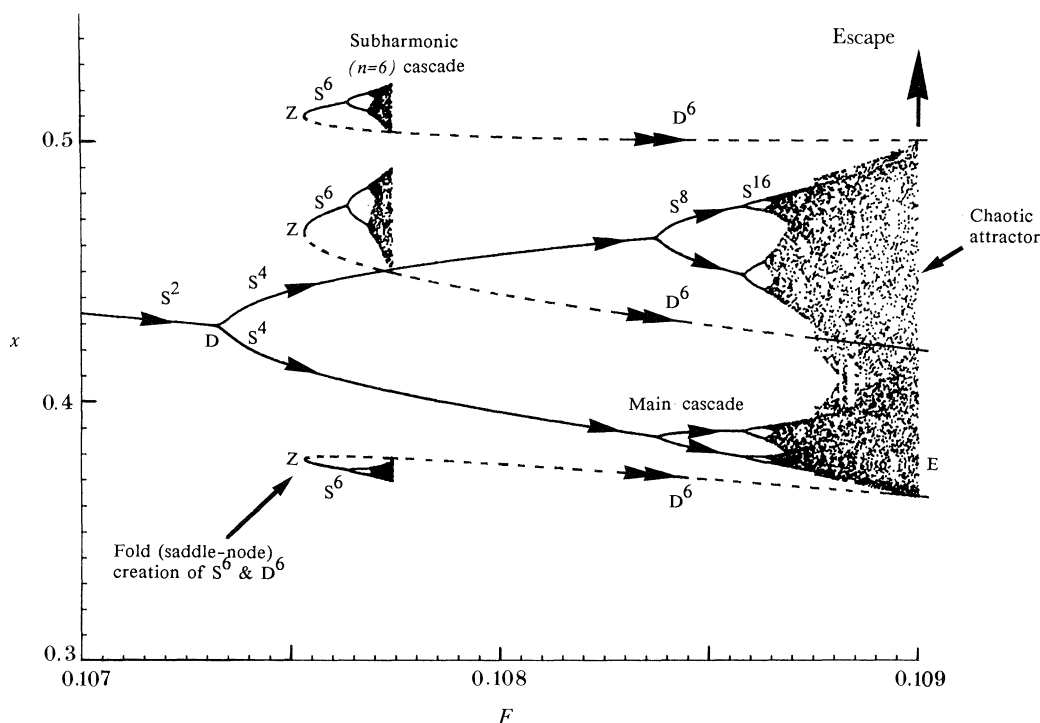
Figure 3. The final steady-state escape mechanism at $\omega = 0.85$ and $\beta = 0.1$. Here x is sampled at twice the driving period and at a phase of $\phi = 180°$. Escape is at the blue sky catastrophe at which the main sequence chaotic attractor collides with D^6, a directly unstable subharmonic oscillation of order 6 created at the fold Z.

Some steady-state responses of the driven system are summarized in figure 2, which shows plots of x, stroboscopically sampled at the forcing frequency, against F, for four values of ω. The linear viscous damping is held constant at $\beta = 0.1$, corresponding to a damping ratio of $\zeta = 0.05$, a fairly realistic value for the rolling of a ship.

In the lower diagram, with $\omega = 0.95$, we see a continuous curve corresponding to a path of steadily growing ($n = 1$) harmonic oscillations of period $2\pi/\omega$ under slowly incremented F. This finally splits into two with the onset of a subharmonic oscillation of order $n = 2$ (period $4\pi/\omega$) at a period-doubling flip bifurcation at C. This is followed by an infinite cascade of flip bifurcations, generating subharmonics of infinitely high order, a chaotic attractor, and finally escape out of the well at E. This scenario persists at the lower values of ω but with the addition of a hysteresis loop, that under slowly varied F at $\omega = 0.85$ would give two jumps (to resonance at fold A, off resonance at fold B) as indicated by the arrows. Meanwhile the progressive retreat of the chaotic bifurcation E to lower F values means that at $\omega = 0.8$ the escape is directly from fold A as indicated. Optimal escape, at the lowest possible value of F, is associated with a codimension-two bifurcation involving the coincidence of E and A at a value of ω just above 0.8. A detailed study of this local-global event is presented by Stewart *et al.* (1990).

This optimal escape corresponds to resonant capsize under lowest possible waves, and is clearly of particular importance. Our detailed study at $\omega = 0.85$, close to this optimum, is therefore of practical relevance.

Figure 3, whose details need not concern us here, is based on data kindly supplied by Y. Ueda, and is taken from Thompson (1989). It shows the remarkable complexity at the end of the period-doubling cascade. Here D is the second period-doubling bifurcation at which S^2, the subharmonic of order $n = 2$ generated at C, flips to give S^4, a subharmonic of order $n = 4$. The final escape is triggered by the collision of the main-sequence chaotic attractor with a directly unstable subharmonic oscillation of order $n = 6$, itself the remnant of a localized fold–cascade–crisis scenario. This final chaotic blue sky catastrophe cannot be predicted by any techniques of classical analytical dynamics.

Steady-state chaotic motions of a more realistic boat model have been identified by Virgin (1987).

Basin erosion and its quantification

The basins of attraction of the stable attracting steady states in the space of the starting values of displacement, $x(0)$, and velocity, $y(0)$, can be determined by a variety of computational techniques. The simplest is a grid of starts, numerical time integrations being simply run from a fine grid and the outcome, escape or non-escape, recorded. A more sophisticated technique is to run time backwards from a ladder of starts along the incoming eigenvector of the unstable hill-top saddle cycle to map out the inset which is the separatrix defining the basin boundary: a sophisticated and highly successful algorithm for this is given by Alexander (1989). Basins can also be computed economically using Hsu's cell-to-cell mapping techniques (Hsu 1987).

Figure 4 shows a sequence of safe basins, from which the system does not escape within $m = 16$ forcing cycles, at $\omega = 0.85$. The pictures are separated by equal F intervals, and the final steady-state escape at $F^E = 0.109$ corresponds approximately to the last picture: the fact that not all trajectories have escaped at $F = 0.110$ is a consequence of the finite duration ($m = 16$) of the simulations. The steady state Poincaré mapping points of the main sequence attractors (obtained by stroboscopically sampling both x and y) are marked on the basins, those shown being all $n = 1$ harmonic motions. The single point displayed in the region of resonant hysteresis is that which would be observed physically under slowly increasing F: the sudden change in position of the mapping point between $F = 0.06$ and $F = 0.07$ is the manifestation of the jump to resonance at $F^A = 0.069$. The ultimate period-doubling cascade, starting at $F^C = 0.1005$, lies entirely between the last two pictures.

The major discovery of our work on the canonical escape equation (Thompson 1989; Soliman & Thompson 1989) is the dramatic sudden erosion of the safe basin, apparent here as we pass from $F = 0.07$ to $F = 0.08$, due to incursive fractal fingers which striate the entire basin.

This behaviour is quantified in figure 5 which shows the variation with $f \equiv F/F^E$ of the area of the safe basin lying within an appropriate (x, y) window. The region of resonant hysteresis is indicated, together with the value of $F^T = 0.0633$ at which there is a homoclinic tangency between the inset and the outset of the hill-top saddle cycle (Thompson 1989). This tangency, which can be predicted accurately by a Melnikov perturbation analysis, signals the appearance of a homoclinic tangle and an associated fractal basin boundary with the infinitely fine recurrent structure of a Cantor set (Thompson & Stewart 1986; Moon 1987; McDonald *et al.* 1985).

The first manifestation of this fractal boundary in figure 4 is the thin finger at $F = 0.070$, but recurrence arguments prove that at any value of F after the tangency there must be an infinity of such fingers: so, although at the resolution of our grid
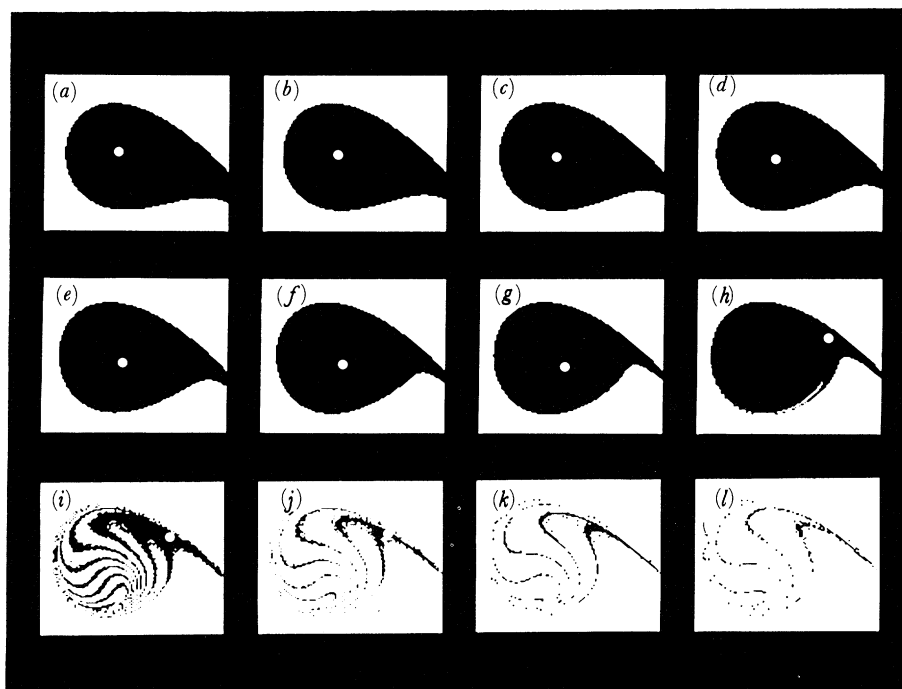
Figure 4. Erosion of the safe basin of the canonical escape equation under increasing F in the window $-0.8 < x < 1.2$, $-1.0 < y < 1.0$. Parameters are $\omega = 0.85$, $\beta = 0.1$, $m = 16$, and the phase is $\phi = 180°$. F increases in steps of 0.01 from 0 in (a) to 0.11 in (l).
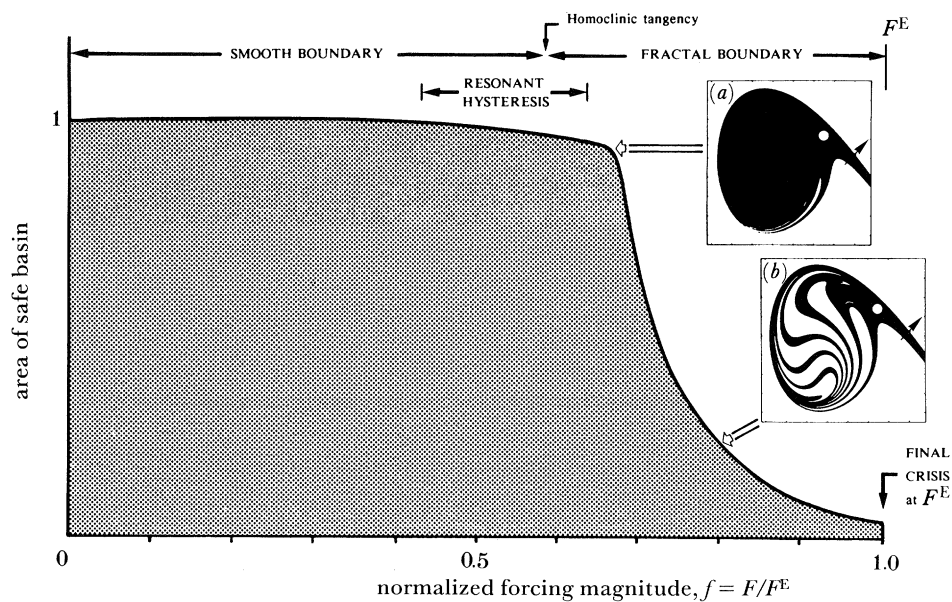

Figure 5. Integrity diagram showing the erosion of the area of the safe basin under increasing F at $\omega = 0.85$, $\beta = 0.1$. Insets: (a) $F = 0.0725$; (b) $F = 0.0872$.
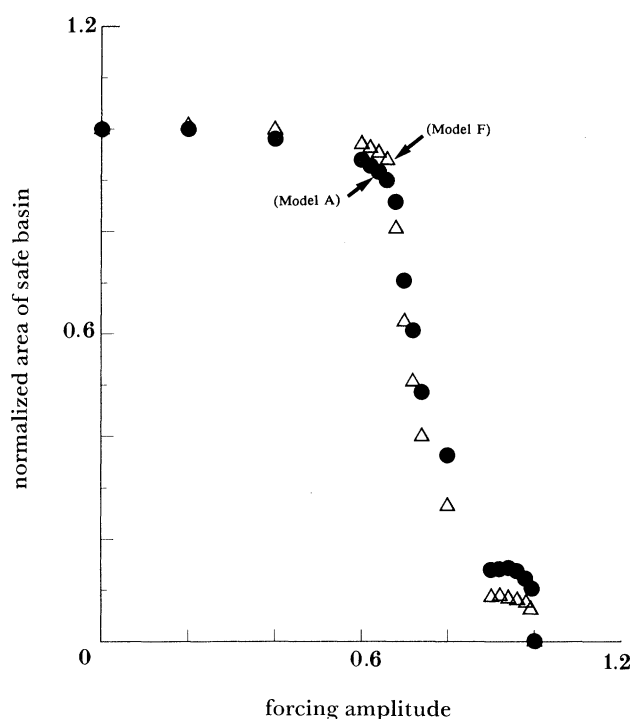
Figure 6. Comparative integrity curves for oscillators with quadratic (model F) and cubic (model A) GZ curves. The forcing amplitude is normalized to unity at the final escape. Damping ratio, 0.05; frequency ratio, 0.85. Results courtesy of Alexis Lansbury.

there appears to be only a single finger at $F = 0.070$, increasing magnifications of the basin boundary would reveal an infinity of finer and finer whiskers. This fractal boundary is only serious from a practical point of view if it becomes incursive and invades the centre of the basin, as it clearly does at $F = 0.080$, giving the cliff-like reduction in area of figure 5.

It is the complete incursive striation, coupled with the sharpness of the cliff, at the relatively low value of $f \approx 0.7$, that makes this phenomenon of great significance to engineers of many disciplines, including naval architecture. Alternative ways of quantifying the loss of engineering integrity, by using, for example, the distance of the steady-state attractor from its basin boundary, or the sensitivity of the attractor to external superimposed noise, are explored by Soliman & Thompson (1989, 1990a).

Robustness under variation of the GZ curve

A vital question clearly centres on the robustness of the phenomenon under changes in the GZ characteristics, and we have recently investigated this (Lansbury & Thompson 1990) using the twin well oscillator which we refer to as model A. As we have noted, this corresponds to the restoring moment of equation (3) with $\alpha = -0.5$. This again represents a biased boat that can only capsize in the direction of positive x, and the change from a quadratic to a cubic GZ introduces a small perturbation in the restoring function. The vanishing of the cubic at $x = 2$, outside the range of current interest, is irrelevant here.
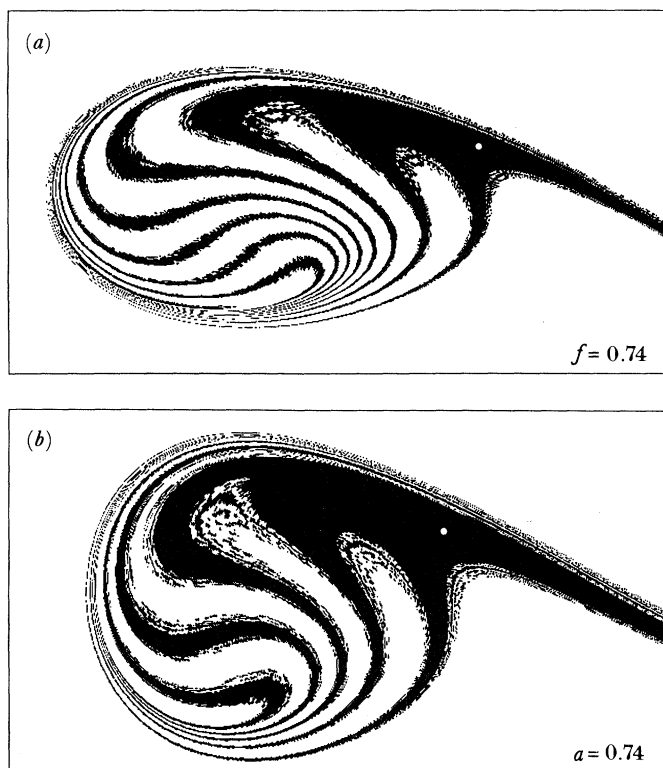
Figure 7. Comparative safe basins for (*a*) model F and (*b*) model A using a cell-to-cell algorithm courtesy of A. McRobie. Cell grid of 640×350 is synchronized with the screen pixels of an IBM PC. Damping ratio 0.05; frequency ratio 0.85.

Taking identical values for the damping ratio and the frequency ratio this study has obtained the very remarkable quantitative correlation of figure 6 for the erosion of the safe basin. Here the forcing amplitude is in both cases normalized to unity at the final escape value, eliminating the need for an arbitrarily defined forcing ratio.

The mechanism of erosion of model A ($\alpha = -0.5$) is, moreover, qualitatively similar to that of our canonical model F ($\alpha = 0$), with incursive fractals striating the entire basin as shown in figure 7. These pictures were obtained using Hsu's cell-to-cell mapping technique with 640×350 cells synchronized with the pixels of an IBM PC. The forcing magnitude is in each case 0.74 times that of the final escape.

The remarkable similarity of behaviour in these mathematically distinct oscillators suggests that sudden basin erosion by incursive fractals is indeed a robust phenomenon under conditions of near-optimal escape.

Role of the damping level

It remains to study the influence of damping on the basin erosion, and we present an analysis of a linear system in the Appendix. This system is assumed to fail (capsize) if x exceeds one, and the size of the safe basin is shown to depend predominantly on just the single detuning:damping ratio given by

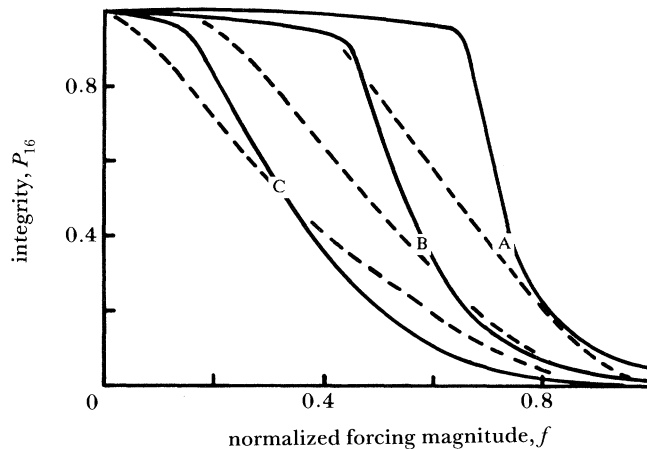$$d = (\omega_f - \omega_n)/\zeta\omega_n, \tag{5}$$

Figure 8. Comparison of the integrity diagrams at three damping levels for nonlinear and linear oscillators. The normalized integrity measure, P_{16}, represents the normalized area of the safe basin. Systems are the canonical escape equation and its linearization, with $\omega = 0.85$. Curves A: $\beta = 0.1$, $d = -3$. Curves B: $\beta = 0.05$, $d = -6$. Curves C: $\beta = 0.01$, $d = -30$. ——, nonlinear; ---, linear.

ω_n being in the present context equal to unity due to our choice of time scale. The safe basin is moreover shown to maintain its original area up to a value of $f = p^c$ where

$$p^c = (1 + d^2)^{-\frac{1}{2}}. \tag{6}$$

For the relatively high values of d of interest at the moment, we can moreover ignore 1 in comparison with d^2 to obtain the approximate relation

$$p^c \approx 1/d = \zeta\omega_n/(\omega_f - \omega_n), \tag{7}$$

showing that at fixed frequencies, p^c scales as the damping ratio. These results are not expected to carry over quantitatively to the nonlinear problem, but do offer a framework for the presentation of results.

Direct computer simulations of our canonical nonlinear oscillator (4), and its linear counterpart obtained by striking out the x^2 term and deeming failure if $x = 1$, yield the integrity curves of figure 8 for three damping levels. Here the integrity measure P_{16} is the proportion of points from a grid of starts which do not fail within 16 forcing cycles, normalized to unity at zero forcing: it is a good measure of the safe basin.

As we would expect from our linear study, the effect of decreasing the damping coefficient β in our nonlinear equation (with ω constant at 0.85) is to give an earlier but less severe erosion. There is, indeed, one theoretical result from our nonlinear studies that reinforces the trend suggested by (7). The onset of fractal basin is predicted by Melnikov's perturbation theory to be at a value of F given by

$$F^M = \beta \sinh(\pi\omega)/5\pi\omega^2, \tag{8}$$

and to the extent that the nonlinear cliff-top occurs just beyond F^M we again have a direct scaling with β. We cannot carry this result over into the normalized diagram with abscissa $f = F/F^E$, however, because we have no knowledge of how the steady state escape value, F^E, scales with the damping.

It may well be that for the best linear to nonlinear correlation the detuning $\Delta\omega = \omega_f - \omega_n$ should be measured not from the linear ω_n but from a lower notional

nonlinear value that acknowledges the softening action of finite amplitudes. We shall not pursue this here, but simply note that quite irrespective of any d correlations, the nonlinear integrity curves always exhibit a much more dramatic cliff-like feature. Indeed it could perhaps be said that the nonlinearity, rather than being the cause of erosion, serves to shore-up the top of the cliff, giving a delayed but necessarily more precipitous eventual decline.

Discussion and Conclusions

Having studied a simple rolling model with different GZ characteristics and different damping levels, we conclude that basin erosion by incursive fractals is a robust phenomenon. This is further confirmed by companion studies of two real ships, the *Edith Terkol* and the *Gaul*, whose dynamic parameters have been well documented following their unexpected capsizes (Soliman & Thompson 1990*b*).

We think, therefore, that transients basins can offer a remarkably simple and repeatable index of capsizability. It can additionally be argued, as in the following three paragraphs, that they might represent a worst-case scenario, but our contribution is in no way dependent on this viewpoint. This is because they certainly represent a more realistic scenario than the one presently used by naval architects in the design office, which, being based solely on the GZ curve, essentially corresponds to still water!

Although sea-states and ocean waves are essentially random processes (but not necessarily stationary ones), a short train or pulse of regular waves that can excite resonant motions may be viewed as a worst-case scenario when considering capsize. For practical purposes, a long train of regular waves can be assigned a probability of zero.

Despite this, most researchers in the extensive literature on ship capsize under regular forcing focus on just the single predominant steady-state motion, be it harmonic, subharmonic or even chaotic. In this, they follow the tradition of classical analysis, despite the fact that for a boat, with its relatively light damping, regular waves will manifestly never persist long enough for transients to decay substantially. Not only is steady-state analysis irrelevant, for this reason, but we have seen that it is also grossly non-conservative.

To deal adequately with a short pulse, we must clearly look at transient motions, and since the starting conditions of a boat at the beginning of the pulse may vary widely, and are in any event unknown, we must look at all possible transient motions. In other words we must adopt the global view of Poincaré's geometrical dynamics (Thompson & Stewart 1986) and inspect the ensemble of all possible motions, rather than focus obsessively on the steady states. In doing this we are likely to get a more robust result that will persist under small irregularities in the forcing.

The simplest and most direct way to do this is to take a grid of starts in the space of the starting conditions of roll angle θ_0 and roll angular velocity θ_0'. Running a simulation from each grid point, we can easily map out in (θ_0, θ_0') space the safe basin from which transient motions do not lead to capsize within the specified duration of the pulse.

The final objective will naturally be to determine a domain of safe operations in the control space of wave height, H, against wave frequency, w, so at each w, for example, the designer needs to specify a safe H. Resonant phenomena will inevitably

focus greatest attention on w values close to w_n, the natural roll frequency of the vessel, the minimum of $H(w)$ being usually just below w_n due to the softening nature of the restoring moment.

At such frequencies, we have shown that the area of the safe transient basin, $A(H)$, falls dramatically at a steep cliff at H^t which can be a small fraction of H^s, the forcing at which the final attracting steady state loses its stability. Clearly H^t should be adopted in preference to H^s in defining the operational locus in the (H, w) domain. We feel that the resulting $H^t(w)$ locus delineating the sea-states of safe operations, will be a valuable new tool in the quantification of the stability of vessels at sea. Rainey & Thompson (1990) have indeed already drawn the attention of naval architects to the practical implication that such a transient capsize diagram, which in operational terms might look like figure 9, can be constructed from such a programme of simulations to give a well-defined measure of 'capsizability' clearly superior to the time-honoured but arbitrary stability criteria based solely on the GZ curve.

Using the robust grid-of-starts technique, a safe basin study is easier to perform, and at the same time more relevant than steady-state analysis. Indeed, as we have seen, our recent studies show that the steady states undergo infinite cascades of period-doubling flip bifurcations, generating subharmonics of arbitrarily high order and ultimately a chaotic attractor whose loss of stability cannot be located by conventional analysis. This high level of dynamic complexity could never be unraveled in routine investigations, and the final steady-state instability is in any case extremely non-conservative when judged against the proposed safe basin criterion.

The dramatic loss of safe-basin area, $A(H)$, occurs after the basin boundary has become fractal (infinitely textured) at H^T, due to a homoclinic tangling of invariant manifolds within the underlying dynamics (Thompson 1989). Starts within this fractal zone lead to chaotic transients, which oscillate hesitatingly for an arbitrary and unpredictable length of time before the boat either capsizes or settles to a safe condition of steady-state harmonic rolling.

This phenomenon is not in itself serious, provided that the fractal zone to which it is confined remains as a thin layer around the edge of the basin, as it does for H just above H^T. However, our studies have shown that as H is further increased the fractal boundary soon becomes incursive with thick finger-like striations penetrating into the very heart of the central zone around the origin $\theta_0 = \theta_0' = 0$. Once this has occurred, the vessel is clearly in an unpredictable and therefore dangerous state.

It is this sudden incursive penetration that causes the well-defined loss of area at H^t, so to pin-point the latter we do not need to use a massive grid of starts but can make just a small number of trial simulations (or model tests) in which a ship in relatively calm water suddenly encounters a train of large regular waves: if the wave height is below the level corresponding to the cliff the ship will remain upright; if it is above it, the ship will capsize repeatably. Indeed a trial simulation from the ambient state at the origin will often be adequate to locate the cliff at H^t with sufficient precision for practical purposes (Thompson & Soliman 1990). Our studies show moreover, that despite the unpredictability of chaotic transients, simulations need only be continued for about 16 wave periods: at a pragmatic engineering level, if a boat does not capsize in 16 forcing cycles it is unlikely to capsize at all.

Requiring, then, perhaps only a single simulation from an ambient start at each (H, w) sea-state, we have a feasible investigation for either computer studies (see, for
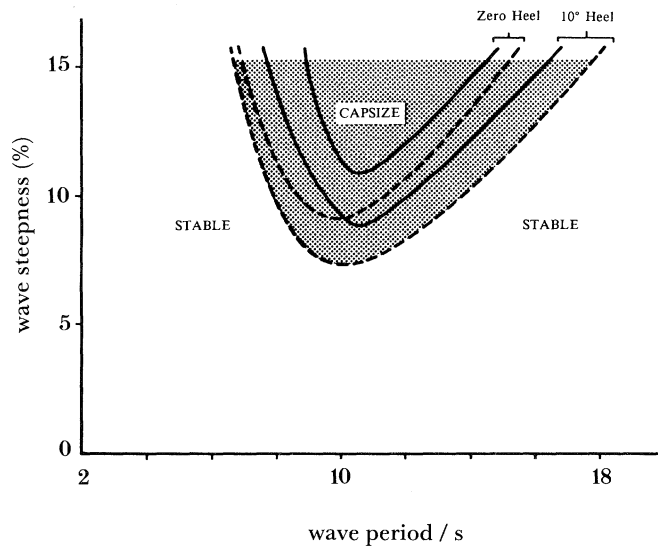
Figure 9. A schematic transient capsize diagram showing how the concepts might be presented in operational terms. ———, quartering seas; – – –, beam seas.

example, Miller *et al.* 1986) or model testing in a wave tank, an investigation that offers distinct advantages over one based on the outdated and narrow concept of steady-state rolling motions.

For practical application, the realism of the nonlinear spring–mass–damper model of ship dynamics would of course be under scrutiny: fortunately, recent developments in hydrodynamic strip theory (Rainey 1989, 1990) promise much more realistic yet still economic simulations. In any event, the generality of the homoclinic tangency mechanism of basin destruction that we have described means that the above transient testing procedure should be equally satisfactory for physical model tests. Hitherto the standard model wave-tank procedure has been to test for capsize in irregular waves of known spectrum, requiring very long experiments, which even then have frequently not produced any capsizes at all (see, for example, Morrall 1981), because sufficiently steep waves occur so rarely in standard sea spectra.

To make a rational assessment of capsizability in either computer simulations or model tests it is indeed necessary to induce a large number of capsizes. In this respect we can draw an instructive parallel with the elastic and plastic approaches to structural safety and collapse. Operational simulations under realistic levels of stochastic forcing are necessary to assess expected roll angles, which must be acceptably low for servicability and passenger safety: these correspond to elastic analyses of working stresses and deflections. By comparison, capsize simulations, under severe and statistically rare wave excitation, test the ultimate resistance to capsize, akin to plastic collapse analysis. We feel that our new transient capsize approach, like plastic mechanism analysis of portal frames, is both easier and more relevant than alternative procedures.
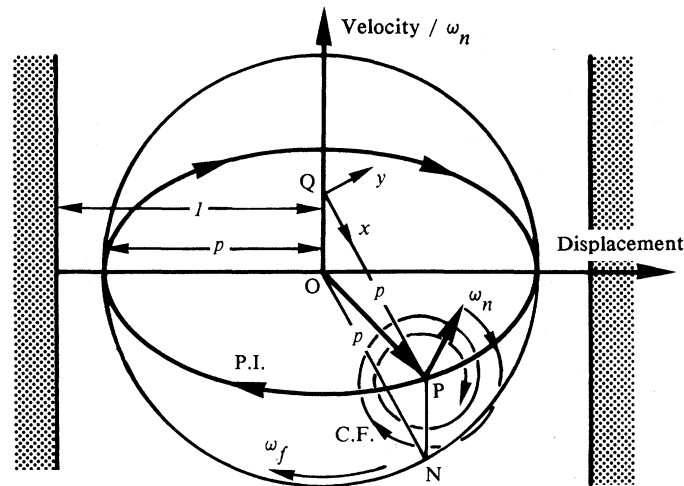
Figure 10. Phase-space representation of the response of a forced linear oscillator, in terms of the particular integral and complementary function vectors.

Appendix. Some linear insights using a rotating frame of reference

The transient behaviour of a linear driven oscillator, as might for example be obtained by deleting the x^2 term from our equation (4), can supply some useful insights and reference curves of basin erosion if we deem it to have failed whenever x exceeds one. To model an asymmetric problem we could specify failure if $x > 1$, while to simulate a symmetric equation we could specify failure if $|x| > 1$. The analysis we present gives the same answer for either case, but the approximation will work less well for the asymmetric case.

The transient behaviour of our linear system can be simply visualized in the phase space of figure 10 as the vector sum of the particular integral (PI) representing the final steady state response to the harmonic excitation, plus the complementary function (CF). The scaling of the velocity axis is chosen to make the unforced, undamped vibrations circular, so the PI describes an elliptical path which is constructed geometrically from the circle swept out by N at the forcing frequency ω_f. The radius ON is of length p, which is proportional to the strength of the forcing and is adopted as a convenient control parameter. Meanwhile the CF decays to zero as a spiral at the natural angular frequency ω_n with a decay rate corresponding to the damping ratio ζ, assumed small. Focusing on the symmetric problem, failure (capsize) is deemed to occur if the resultant of the two vectors crosses into one or other of the shaded areas of the figure.

A convenient device for studying the properties of the safe basin is to adopt the viewpoint of an observer rotating and translating with the axes Qxy, where QP, of length p, is parallel to ON. The angular velocity of these axes is the constant ω_f, and in this rotating frame the shaded failure areas appear as two half-planes rotating in the opposite direction at the harmonic excitation frequency. Because they continuously touch a circle of unit radius centred on Q, they will appear to cover all but this area as they rotate, as shown in figure 11. Meanwhile the complementary function appears as a decaying circular spiral, but instead of taking a time $2\pi/\omega_n$ per
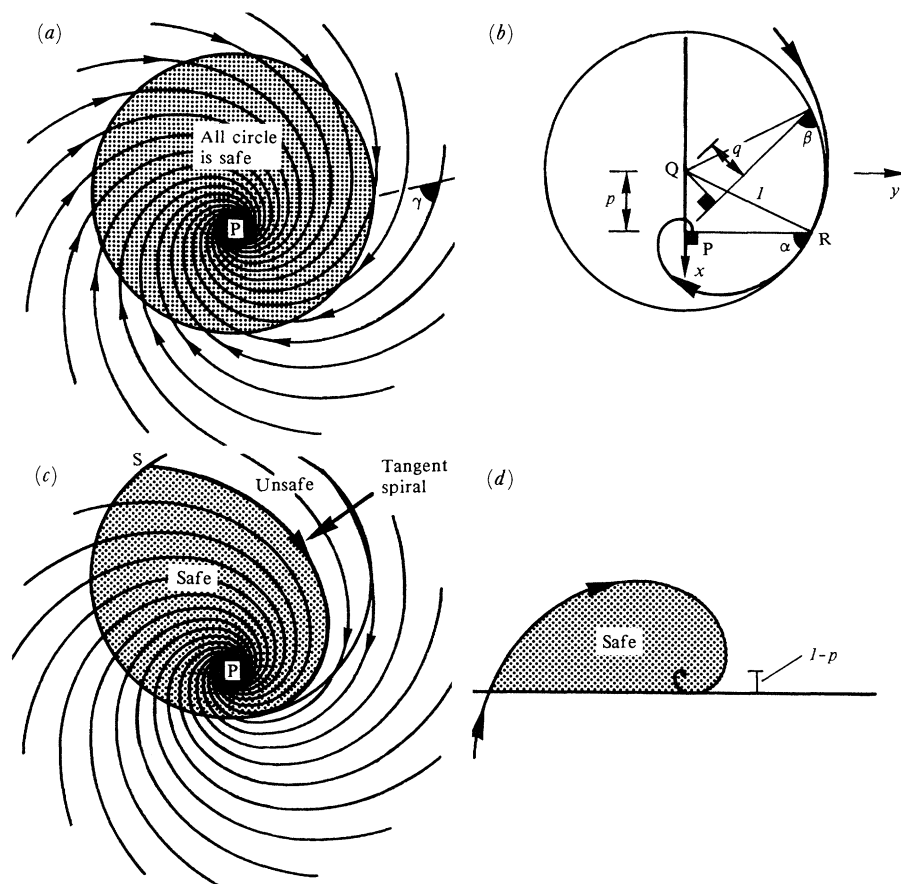
Figure 11. Trajectories of a linear system viewed in a rotating reference frame, showing the progressive erosion of the safe basin. $p^c = \cos\gamma = \cos(\arctan d) = (1+d^2)^{-\frac{1}{2}}$. (a) $p < p^c$, (b) $p = p^c$ (first tangency), (c) $p > p^c$, (d) $p \approx 1$ (this shows a blow-up of the parabolic limit; the circle appears as a straight line; and the area scales as $(1-p)^2$, giving parabolic beach).

revolution, it will now take $2\pi/\Delta\omega$ in terms of the detuning $\Delta\omega \equiv \omega_f - \omega_n$. During this time it will have decayed by a factor $\exp(2\pi\zeta\omega_n/\Delta\omega)$ rather than merely $\exp(2\pi\zeta)$, so that for a small detuning ratio $\Delta\omega/\omega_n$ the spiral will appear to contract much more steeply, as illustrated.

Now the spiralling trajectory of a damped unforced oscillator is never a true spiral with a constant angle between the trajectory and the radius vector, but can be approximated as such if the damping is light. Under the rotation of the reference frame, a true spiral will remain a true spiral, with, however, a change in the constant angle. From these considerations we can conclude that in our rotating frame of figure 11, the angle of the spiral, denoted by γ in figure 11a, is given by $\gamma = \arctan d$, where $d \equiv \Delta\omega/\zeta\omega_n$ is the detuning–damping ratio. Thus, strikingly, the slope of the spiral in the rotating reference frame is controlled as much by the detuning ratio as by the damping. Focusing attention on small values of the detuning ratio, the counter-rotating failure areas will be rotating much faster than the spiral, making failure inevitable whenever the spiralling trajectory strays outside the circle that they mark
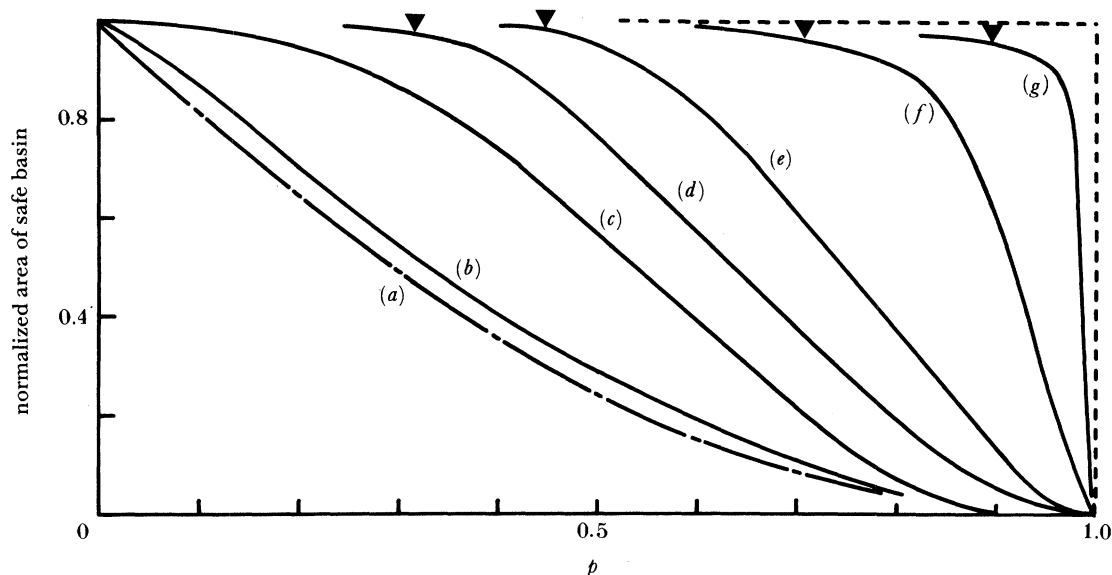
Figure 12. Safe basin plots for the linear system using the single detuning-damping parameter. The first tangency, at p^c, is indicated by a black triangle for four values of d. The values of d are: (a) ∞ (zero-damping parabola); (b) 30; (c) 4; (d) 3; (e) 2; (f) 1; (g) 0.5. - - -, $d = 0$ (zero detuning).

out. We therefore reach the important conclusion that the size of the safe basin at a given value of p will be governed solely by the detuning–damping ratio d, and will not be controlled independently by the detuning and damping ratios themselves.

The corresponding integrity curves are likewise parametrized solely by d, and their characteristics are revealed by a further consideration of figure 11. The problem is to relate the area of the safe, non-failing starts to the forcing level as measured by p, which is the distance from the centre of the spiral, P, to the centre of the unit circle, Q. When this level is small as in figure 11a, trajectories starting anywhere within the circle will safely complete their spiral course, so the basin area remains exactly equal to the area, π, of the circle. At the larger excitation level of figure 11c, however, some spiral trajectories leave the circle and create an unsafe area behind, bounded by the tangent spiral shown. Clearly this starts to happen when there are points on the circle at which the angle β between a tangent and a line to P is less than the characteristic angle, γ, of the spiral. Now with reference to figure 11b we can observe that since $\cos \alpha = p$ and $\cos \beta = q$, the obvious inequality $p > q$ implies $\beta > \alpha$: in other words the minimum value of β occurs at the point R where PR is at right angles to PQ. Hence the first tangency occurs at R when $\alpha = \gamma$ giving the value of p for first erosion of the circle as

$$p^c = \cos \gamma = \cos(\arctan d) = (1 + d^2)^{-\frac{1}{2}}. \tag{A 1}$$

We notice here that the sign of d (i.e. the sign of $\Delta\omega$) is irrelevant, figures 10 and 11 having been drawn, arbitrarily, for the case of $\Delta\omega$ negative.

Beyond this critical 'cliff-top' value, the area of the safe basin decays progressively with p, as it becomes increasingly bounded by the tangent spiral, whose intersection, S, with the circle moves round anticlockwise in figure 11c as p tends to one.

Approximate trigonometric formulae for the variation of the safe area with p, as

parametrized by d, can be written down, but will not be presented here. It is, however, of interest to look finally at the limiting case as p approaches unity, and the area shrinks to zero. This is illustrated in the blow-up of figure $11d$ where the circle appears as a straight line. Diagrams at different, small values of $1-p$ are therefore self-similar, and the area therefore scales as $(1-p)^2$, giving a parabolic beach at the foot of the cliff.

Direct computer simulations of a linear system, with both symmetric and asymmetric failure criteria, confirm the dominant role of the single detuning-damping parameter, d, the effect of varying the two parameters $\Delta\omega$ and ζ at constant d having only a secondary minor effect on the integrity curves. The results are summarized in figure 12, which shows the curves, parametrized by d between the two limits of $d = 0$ (two straight lines) and $d = \infty$ (a parabola).

The former corresponds to a situation with no detuning. The PI and CF are therefore synchronized, and in the rotating reference frame the trajectories move along straight lines towards P: there is no possibility of a tangency, and the full circle remains the safe basin until P itself passes outside the circle at $p = 1$. The latter limiting case of $d = \infty$ arises when there is no damping. The CF rotates in a circle about P, and the safe area is a shrinking circle of radius $1-p$ and area $\pi(1-p)^2$.

The values of p^c from equation (A 1), corresponding to the first tangency at which our simplified analysis predicts the first decrease in the safe area, are marked by the black triangles. These are seen to be a useful guide to the beginning of the erosion process.

References

Alexander, N. A. 1989 Production of computational portraits of bounded invariant manifolds. *J. Sound Vib.* **135**, 63–77.

Hsu, C. S. 1987 *Cell-to-cell mapping: a method of global analysis for nonlinear systems.* New York: Springer Verlag.

Lansbury, A. N. & Thompson, J. M. T. 1990 Incursive fractals: a robust mechanism of basin erosion preceding the optimal escape from a potential well. *Physics Lett.* (Submitted.)

Lloyd, A. R. J. M. 1989 *Seakeeping: ship behaviour in rough weather.* Chichester: Ellis Horwood.

McDonald, S. W., Grebogi, C., Ott, E. & Yorke, J. A. 1985 Fractal basin boundaries. *Physica* D **17**, 125–153.

Miller, D. R., Tam, G., Rainey, R. C. T. & Ritch, R. 1986 Investigation of the use of modern ship motion prediction models in identifying ships with a larger than acceptable risk of dynamic capsize. Report prepared by Arctec Canada Ltd for the Transportation Development Centre of the Canadian Government. *Rep. no. TP7407E.*

Moon, F. C. 1987 *Chaotic vibrations: an introduction for applied scientists and engineers.* New York: Wiley.

Morrall, A. 1981 The *GAUL* disaster: an investigation into the loss of a large stern trawler. *Trans. R. Inst. Nav. Arch.* **123**, 391–440.

Motora, S. (ed.) 1982 *Proc. 2nd Int. Conf. on Stability of Ships and Ocean Vehicles.* Tokyo: Soc. Nav. Arch. Japan.

Rainey, R. C. T. 1989 A new equation for calculating wave loads on offshore structures. *J. Fluid Mech.* **204**, 295–324.

Rainey, R. C. T. 1990 Energy arguments under a 'wavy lid' – a new approach to capsizing and other highly nonlinear phenomena. In *Proc. 5th Int. Workshop on Water Waves and Floating Bodies* (ed. F. Ursell). Manchester University: Department of Mathematics.

Rainey, R. C. T. & Thompson, J. M. T. 1990 The transient capsize diagram – a new method of quantifying stability in waves. *J. Ship Res.* (In the press.)

Soliman, M. S. & Thompson, J. M. T. 1989 Integrity measures quantifying the erosion of smooth and fractal basins of attraction. *J. Sound Vib.* **135**, 453–475.

Soliman, M. S. & Thompson, J. M. T. 1990*a* Stochastic penetration of smooth and fractal basin boundaries under noise excitation. *Dynamics Stability Syst.* (In the press.)

Soliman, M. S. & Thompson, J. M. T. 1990*b* Transient and steady state analysis of capsize phenomena. *Appl. Ocean Res.* (In the press.)

Stewart, H. B., Thompson, J. M. T., Ueda, Y. & Lansbury, A. N. 1990 (In preparation.)

Thompson, J. M. T. 1989 Chaotic phenomena triggering the escape from a potential well. *Proc. R. Soc. Lond.* A **421**, 195–225.

Thompson, J. M. T. & Soliman, M. S. 1990 Fractal control boundaries of driven oscillators and their relevance to safe engineering design. *Proc. R. Soc. Lond.* A **428**, 1–13.

Thompson, J. M. T. & Stewart, H. B. 1986 *Nonlinear dynamics and chaos.* Chichester: Wiley.

Thompson, J. M. T. & Ueda, Y. 1989 Basin boundary metamorphoses in the canonical escape equation. *Dynamics Stability Syst.* **4**, 285–294.

Virgin, L. N. 1987 The nonlinear rolling response of a vessel including chaotic motions leading to capsize in regular seas. *Appl. Ocean Res.* **9**, 89–95.